PTEN knockdown alters dendritic spine/ protrusion morphology, not density

Citation: Haws, Michael E., Thomas C. Jaramillo, Felipe Espinosa, Allie J. Widman, Garret D. Stuber, Dennis R. Sparta, Kay M. Tye, et al. "PTEN Knockdown Alters Dendritic Spine/protrusion Morphology, Not Density." J. Comp. Neurol. 522, no. 5 (February 12, 2014): 1171–1190.

As Published: http://dx.doi.org/10.1002/cne.23488

Publisher: Wiley Blackwell

Persistent URL: http://hdl.handle.net/1721.1/102670

Version: Author's final manuscript: final author's manuscript post peer review, without publisher's formatting or copy editing

Published in final edited form as:
J Comp Neurol. 2014 April 1; 522(5): 1171–1190. doi:10.1002/cne.23488.

PTEN knockdown alters dendritic spine/protrusion morphology, not density

Michael E. Haws[1,2], **Thomas C. Jaramillo**[1], **Felipe Espinosa-Becerra**[1], **Allie Widman**[1], **Garret D. Stuber**[3], **Dennis R. Sparta**[3], **Kay M. Tye**[4], **Scott J. Russo**[5], **Luis F. Parada**[6], **Michael Kaplitt**[7], **Antonello Bonci**[8], and **Craig M. Powell**[1,2,9]

[1] Neurology & Neurotherapeutics, The University of Texas Southwestern Medical Center Dallas, Texas, 75390-8813

[2] Neuroscience Graduate Program, The University of Texas Southwestern Medical Center, Dallas, Texas, 75390-8813

[5] Neuroscience, Mount Sinai School of Medicine, New York, NY 10029

[6] Developmental Biology, The University of Texas Southwestern Medical Center, Dallas, TX, 75390

[7] Neurological Surgery, Neurology, Otorhinolaryngology, Weill Cornell Medical College, New York, NY 10065

[8] National Institute on Drug Abuse, Intramural Research Program, Bethesda, MD 21224; Dept. Of Neurology, UCSF, San Francisco; Solomon H Snyder Department of Neuroscience and Department of Psychiatry, Johns Hopkins School of medicine, Baltimore, MD

[9] Psychiatry, The University of Texas Southwestern Medical Center, Dallas, Texas, 75390-8813

Abstract

Mutations in phosphatase and tensin homolog deleted on chromosome ten (PTEN) are implicated in neuropsychiatric disorders including autism. Previous studies report that PTEN knockdown in neurons *in vivo* leads to increased spine density and synaptic activity. To better characterize synaptic changes in neurons lacking PTEN, we examined the effects of shRNA knockdown of PTEN in basolateral amygdala neurons on synaptic spine density and morphology using fluorescent dye confocal imaging. Contrary to previous studies in dentate gyrus, we find that knockdown of PTEN in basolateral amygdala leads to a significant decrease in total spine density in distal dendrites. Curiously, this decreased spine density is associated with increased miniature excitatory post-synaptic current frequency and amplitude, suggesting an increase in number and function of mature spines. These seemingly contradictory findings were reconciled by spine morphology analysis demonstrating increased mushroom spine density and size with correspondingly decreased thin protrusion density at more distal segments. The same analysis of

Correspondence and requests for materials should be addressed to C.M.P. (5323 Harry Hines Blvd., Dallas, TX 75390-8813, (214)-633-1880, craig.powell@utsouthwestern.edu).
[3]Present Address: Psychiatry, Cell Biology and Physiology, Neuroscience Center, University of North Carolina, Chapel Hill, NC 27599-7250
[4]Present Address: Dept. Of Brain and Cognitive Sciences, Picower Institute for Learning and Memory, Massachusetts Institute of Technology, Cambridge, MA 02139

Conflict of Interest Statement The authors declare no competing financial interests.

PTEN conditional deletion in dentate gyrus demonstrated that loss of PTEN does not significantly alter total density of dendritic protrusions in the dentate gyrus, but does decrease thin protrusion density and increases density of more mature mushroom spines. These findings suggest that, contrary to previous reports, PTEN knockdown may not induce *de novo* spinogenesis, but instead may increase synaptic activity by inducing morphological and functional maturation of spines. Furthermore, behavioral analysis of basolateral amygdala PTEN knockdown suggests that these changes limited only to the basolateral amygdala complex may not be sufficient to induce increased anxiety-related behaviors.

Keywords

Dendrite; spine; amygdala; dentate gyrus; AKT; mTOR; PTEN

Introduction

Phosphatase and tensin homolog deleted on chromosome ten (PTEN) is a lipid and protein phosphatase that negatively regulates the phosphatidylinositol 3-kinase (PI3K)/AKT/mTOR signaling pathway, ultimately modulating cell growth and translation (Besson et al., 1999; Dahia, 2000; Di Cristofano and Pandolfi, 2000; Downes et al., 2001; Eng, 1999; 2003; Hobert and Eng, 2009; Hoeffer and Klann, 2010; Leslie and Downes, 2002; Maehama and Dixon, 1998; 1999; Orloff and Eng, 2008; Vazquez and Sellers, 2000; Waite and Eng, 2002). *PTEN* was originally discovered as the gene responsible for a subset of familial hamartoma syndromes associated with increased risk for certain cancers (Nelen et al., 1997) and as a gene often mutated in human cancers and tumor cell lines (Li et al., 1997; Steck et al., 1997). More recently, mutations in PTEN have been linked directly to autism with macrocephaly and neurodevelopmental delay with macrocephaly, findings that have been replicated by multiple laboratories in multiple cohorts (Boccone et al., 2006; Butler et al., 2005; Buxbaum et al., 2007; Goffin et al., 2001; Herman et al., 2007; McBride et al., 2010; Orrico et al., 2009; Stein et al., 2010; Varga et al., 2009; Zori et al., 1998). Thus, understanding PTEN's role in neuronal morphology and function is important for understanding human neuropsychiatric disease.

PTEN deficiency results in erratic neuronal migration, neuronal hypertrophy, and abnormal arborization and myelination in humans (Abel et al., 2005) and animal models (Backman et al., 2001; Fraser et al., 2008; Kwon et al., 2006; Kwon et al., 2001; Xiong et al., 2012). Using Golgi staining or immunohistochemistry, we and others have demonstrated that PTEN-deficient neurons in brains of animal models have increased synaptic spine density (Fraser et al., 2008; Kwon et al., 2006; Luikart et al., 2011; Pun et al., 2012; Zhou et al., 2009) and increased frequency of mEPSCs (Luikart et al., 2011), while PTEN overexpression can decrease apparent synaptic spine density (Zhang et al., 2012), findings suggestive of a role for PTEN in *de novo* synapse and synaptic spine formation.

Using sensitive fluorescent dye measures (Dumitriu et al., 2012a; Dumitriu et al., 2010; Dumitriu et al., 2012b; Dumitriu et al., 2011), we have performed a detailed analysis of synaptic spine/dendritic protrusion density and morphology in two different populations of central neurons with shRNA knockdown or transgenic deletion of PTEN. Interestingly, using these methods we do not find an increased dendritic protrusion density, but rather an overall *decrease* in total dendritic protrusion density in basolateral amygdala complex (BLA) neurons associated with a *decrease* in density of thin protrusions at distal dendritic segments and an *increase* in density of more “mature”, mushroom-shaped spines all along the dendritic tree. In the dentate gyrus granule neurons we found no change in overall dendritic protrusion density, but the same shift in protrusion morphology: decreased thin

protrusions and increased mushroom spines. Head diameter of mushroom-shaped spines is also significantly increased. These changes are accompanied by increased frequency and amplitude of mEPSCs onto PTEN-deficient neurons, implying that this structural spine maturation is accompanied by concomitant functional maturation. These results implicate PTEN and the PI3K/AKT/mTOR pathway in functional and structural alterations in dendritic protrusions rather than *de novo* spine formation. Finally, although we cannot completely rule out a role for PTEN in the BLA in anxiety-related behaviors, our data suggest that focal, limited PTEN knockdown and the correlated increased mushroom spine density in the BLA is not sufficient to cause anxiety-like behavioral phenotypes that have previously been correlated with increased BLA spine density and anxiety-like behaviors following chronic stress (Lakshminarasimhan and Chattarji, 2012).

Methods and Materials

Recombinant Adeno-Associated Virus

Viruses were constructed and purified by the laboratory of Dr. Michael Kaplitt. Recombinant adeno-associated virus (rAAV) vectors encoding for luciferase-silencing or PTEN-silencing short hairpin loop RNA (shLuciferase and shPTEN respectively) sequences were generated as follows: DNA oligos encoding shLuc and shPTEN were annealed and cloned immediately downstream from the human PolIII H1 promoter into *Bgl*II and *Xba*I sites of an rAAV vector. The following oligos were used: 5'-GATCCCCCCGCTGGAGAGCAACTGCATTTCAAGAGA ATGCAGTTGCTCTCCAGCGGTTTTTGGAA-3' (shLuc) and 5'-GATCCCCGAGTTCTTCCACAAACAGAACTTCCTGTCA TTCTGTTTGTGGAAGAACTCTTTTTTGGAAT-3' (shPTEN). The underlined regions are the target-specific palindrome sequences separated by the loop sequence. The rAAV vector bicistronically expresses YFP under the control of the hybrid CMV enhancer/chicken β-actin promoter. Vector stocks were prepared by packaging the plasmids into AAV serotype 2 particles using a helper-free plasmid transfection system. Serotype 2 has been shown to have specificity for neurons over microglia and astrocytes (Bartlett et al., 1998). The vectors were purified using heparin affinity chromatography and dialyzed against PBS. AAV titers were determined by quantitative PCR using CMV-enhancer-specific primers and adjusted to 10^{11} genomic particles per ml. The integrity and accuracy of all constructs were verified by sequencing.

Intracranial viral injections

7 week old male C57BL/6J mice were anesthetized with 0.1 ml of a 20% ketamine, 10% xylazine in 0.9% saline solution, mounted onto a mouse stereotactic apparatus (KOPF Instruments, Tujunga, CA), and sterilized with ethanol and povidone-iodine (Betadine, Purdue Products). Holes in the skull were drilled 1.2 mm posterior, 3.25 mm lateral from bregma bilaterally and a pulled glass capillary pipette (Sutter Instruments, Novato, CA) containing the virus was brought to the brain surface. The pipette was lowered 4.5 mm where 0.5 μl of AAV-shPTEN or AAV-shLuc was slowly injected into the region of the basolateral amygdala complex (BLA – comprised of the basolateral and lateral nuclei of the amygdala). Following injections, silk sutures were used to close the wound. The location and spread of viral infection was examined post-mortem using immunohistochemistry (IHC – method described below) to detect YFP expression. Only mice that bilaterally expressed YFP in the BLA without significant YFP expression in the cortex, striatum or central amygdala were defined as bilateral BLA hits and used for experimental analysis. This determination took place after the experiments were completed by an investigator blind to the experimental results of each individual mouse. On a randomly chosen, representative subset of the same mice that had undergone viral injections and behavioral testing, we used

IHC on 30 μm thick brain sections to co-localize the neuronal marker NeuN with virally expressed YFP, and then took high magnification images within an infected region of the BLA. The percentage of neurons infected was then calculated as the percent of NeuN+ cells that were also YFP+. N=3 animals from which 5 slices were analyzed from each mouse and averaged together. Immunohistochemical, electrophysiological, and morphological experiments were performed 3 weeks after surgeries. All experiments were done in accordance with NIH (National Institutes of Health) and University of Texas Southwestern Medical Center animal guidelines and protocols.

Immunohistochemistry

Virus-injected mice were perfused with 4 % paraformaldehyde (Sigma; St. Louis, MO), then whole brains were post-fixed in 4 % paraformaldehyde at 4°C overnight. Brains were then transferred to 30 % sucrose (Sigma) and allowed to equilibrate until they sank. 30 μm sections were cut (HM 430 Sliding microtome, Microm; Waldorf, Germany) at dry ice temperatures and stored at 4°C in PBS containing 0.1 % sodium azide (Sigma) until use. Tissue sections were mounted onto positively charged glass slides (Fisher; Waltham, MA) and allowed to air dry. A 0.1 M citric acid (Sigma) antigen unmasking treatment was performed prior to blocking slices with 3 % normal donkey serum (NDS) (Jackson ImmunoResearch; West Grove, PA) in PBS containing 0.3 % triton X-100 (Sigma). Overnight primary antibody incubation in 3 % NDS, 0.3 % Tween-20 (Sigma) in PBS at room temperature was followed by a 2 h secondary antibody treatment. Tyramide amplification was performed using the Avidin Biotin Complex Kit (Vector Laboratories; Burlingame, CA) and a Tyramide Signal Amplification Kit (PerkenElmer; Waltham, MA). Images were taken on an Olympus BX51 epifluorescent microscope (Tokyo, Japan).

Antibody Characterization

Primary antibody details, sources and their concentrations are shown in Table 1. Secondary antibodies used were FITC-conjugated donkey anti-chicken, FITC-conjugated donkey anti-rabbit, CY3-conjugated donkey anti-mouse and Biotin-conjugated donkey anti-rabbit (Jackson ImmunoResearch, West Grove, PA).

The rabbit anti-GFP antibody (Invitrogen, Carlsbad, CA) recognizes the gene product of GFP-expressing transgenic mice and is not reactive with non-GFP expressing mice (Moldrich et al., 2010). In the current study, staining was only observed in brain regions infected with either shPTEN or shLuc which express the *Aequorea victoria* fluorescent protein color variant YFP.

The chicken anti-GFP antibody (Aves Labs, Tigard, OR) recognizes the gene product of GFP-expressing transgenic mice and is not reactive with non-GFP expressing mice (Encinas et al., 2006), and the specificity has been verified by the manufacturer by Western blot. In the current study, staining was only observed in brain regions infected with either shPTEN or shLuc which express the *Aequorea victoria* fluorescent protein color variant YFP.

The mouse anti-NeuN (Millipore, Billerica, MA) antibody recognizes the DNA-binding neuron-specific protein NeuN, which is present in most neuronal cell types of vertebrate CNS. It does not stain non-neuronal cell types. It stains only nuclei in a neuronal pattern consistent with previous findings in the mouse brain (Mullen et al., 1992).

The rabbit anti-PTEN antibody (Cell Signaling Technology Inc., Danvers, MA) recognizes phosphatase and tensin homolog (PTEN) protein. Specificity of this antibody was shown by Western blot using whole cell lysates of the endometrial cancer cell line Hec-1b with wild-type PTEN and of the breast cancer cell line MDA-MB-415 harboring a PTEN mutation. No

PTEN immunoreactivity was observed in the mutant line by Western blot (Forster et al., 2011). The specificity has also been verified by the manufacturer by Western blot using HeLa, COS-7 and C6 cell lines.

The rabbit anti-pAKT antibody (Cell Signaling Technology Inc., Danvers, MA) recognizes the akt protein when phosphorylated at serine 473. Specificity for phosphorylated Akt was shown by the manufacturer by Western blot. When PC-3 cells were pretreated with LY249002 and Wortmanin, the immunoreactive band at ~62 kD is absent while the antibody is immunoreactive with untreated PC-3 cells.

Neuronal Morphology and Dendritic Protrusion Density

Basolateral Amygdala Neurons—Mouse brain tissue was prepared for intracellular loading of neurons in the BLA with Alexa Fluor 568 following methods reported by Dumitriu, et al., with minor modifications (Dumitriu et al., 2010; Dumitriu et al., 2011). Mice used for dendritic protrusion analysis were injected with virus and then sacrificed between 21–25 days later. Mouse injections were staggered so that we could sacrifice 2 mice at a time (1 shLuc and 1 shPTEN), allowing for perfusion, cell filling and confocal imaging to be done within 72 hours. Virus-injected mice were perfused with 5 ml of 1 % PFA in 0.1 M phosphate buffer, pH 7.4 (PB) followed by 60 ml of 4 % PFA and 0.125 % Glutaraldehyde in 0.1 M PB at 5 ml/min. Brains were post-fixed for 2 hours in 4 % PFA and 0.125 % Glutaraldehyde in 0.1 M PB then 225 μm thick slices were cut on a vibratome in chilled 1X PBS (Fisher, Waltham, MA) and stored in 1X PBS at 4°C until use.

Loading of virally infected neurons with Alexa Fluor 568 (Invitrogen) was performed as previously described (Hao et al., 2006) with minor modifications. Sections were immersed in 1X PBS and virally infected neurons of the BLA were identified by epifluorescence, impaled with sharp micropipettes, and loaded with 10 mM Alexa Fluor 568 in 200 mM KCl under a direct current of 1–4 nA for 5–10 min, or until the dye filled distal processes and no additional loading was observed. 5–10 neurons were loaded with dye per mouse and 2–4 neurons were loaded per slice. Sections containing loaded cells were mounted on glass slides, and covered with H-1000 Vectashield mounting medium (Vector Laboratories). Confocal z-stacks of filled neurons contained 50–80 images 2 μm apart and were captured with a Plan-Achromat 20X/0.75 NA objective lens on a Zeiss, LSM 510. Filled neurons had to meet four criteria to be kept for morphological and dendritic protrusion analysis. (1) The neuron had to be located in the basolateral amygdala complex. (2) The neuron had to express YFP, detected with 3-dimensional imaging taken by confocal fluorescent microscopy (Laser Scanning Microscope 510, Zeiss, Peabody, MA). (3) Due to differences in morphology and dendritic protrusion density between different neuron types in the BLA, the neuron had to be a Class I neuron (McDonald, 1982). Class I neurons were defined as cells with a soma at least 15 μm in diameter, at least 5 primary dendrites and at least 3 quaternary branches derived from different primary branches. (4) The center of the cell body had to be located 20–35 μm beneath the surface of the slice so that a consistent portion of the total dendritic arbor would be included in morphological analysis. 3-dimensional digital reconstructions of neurons were created using Neurolucida and morphological analysis was performed with NeuroExplorer (MBF Bioscience, Williston, VT). After excluding cells that did not meet these criteria, 17 shLuc infected cells from 5 mice and 16 shPTEN infected cells from 5 mice were included in the amygdala study.

Printouts of neuronal reconstructions that included a series of scaled, concentric circles 10 μm apart centered on the cell body were used to pseudo-randomly select dendritic segments for spine/protrusion analysis. We selected one dendritic segment every 10 μm from the cell body up to 100 μm. Confocal z-stacks of dendritic segments containing up to 60 images 0.2 μm apart were captured with a 100X/1.4 NA oil immersion objective lens on a Zeiss, LSM

510. Dendritic segments had to meet three criteria to be imaged and included in analysis. (1) The dendritic segment had to span a 10 μm thick circular band created by two adjacent concentric circles. (2) The dendritic segment had to be nearly parallel to the surface of the slice, such that the entire segment could be imaged within a 6 μm thick z-stack. (3) No branching or crossing of nearby labeled dendrites could be observed within the segment. Settings for pinhole size, aperture gain, and offset were optimized initially and then held constant throughout the study to ensure that all images were digitized under the same illumination conditions at a resolution of 0.032 μm × 0.032 μm × 0.2 μm per voxel. One high magnification image was taken every 10 μm from the soma up to 100 μm from the soma. The confocal z-stacks were deconvolved with AutoDeblur (Media Cybernetics, Bethesda, MD) and imported into NeuronStudio (available for download online at http://research.mssm.edu/cnic/tools-ns.html, Icahn School of Medicine at Mount Sinai, New York, NY) for semi-automated three-dimensional dendrite segment width and length, spine/protrusion density, spine/protrusion head diameter and spine classification analysis as previously reported (Rodriguez et al., 2008; Rodriguez et al., 2006; Wearne et al., 2005). Briefly, the spine/protrusion density was calculated by dividing the total number of protrusions present by the length of the dendritic segment. Spine/protrusion subtypes were characterized using Neuron Studio as follows: A protrusion was deemed stubby if no neck was identified and the total length of the protrusion was < 2.5 times the width of the base of the protrusion. A protrusion was classified as a thin protrusion when no neck was identified but its total length was > 2.5 times the width of the identified base of the spine, or when a neck was identified but the head diameter was < 0.37 μm. A mushroom spine was classified as a spine with a neck and a head diameter > 0.37 μm. Details regarding the algorithms used to calculate head diameter and neck length have been published elsewhere (Rodriguez et al., 2008). Of note, head diameter is taken as the largest diameter of the head in three-dimensional space. The head diameter threshold of 0.37 μm was obtained by manually classifying spines in a subset of shLuc neurons and plotting the head diameter distribution of thin and mushrooms protrusions. The intersection of those distributions was used as the head diameter threshold. No distinction was made between filopodia and thin spines and thus both are included in the thin protrusion category due to difficulties in resolving the difference at the light microscope level. A Student's t-test was used for statistical analysis except when distance was included as a repeated measure factor in which case a 2-way ANOVA with repeated measures was used.

Dentate Gyrus Granule Neurons—$PTEN^{loxP}$ mice (Suzuki et al., 2001) and Nse-cre mice (Kwon et al., 2006) were provided by Dr. Luis Parada and have been characterized in previous reports. Briefly, both lines have been maintained in C57BL/6 inbred background. PTEN mutant mice (Nse–cre;$PTEN^{loxP/loxP}$) were generated by breeding male $PTEN^{loxP/loxP}$ mice and female Nse–cre;$PTEN^{loxP/+}$ mice. Controls used here were $PTEN^{loxP/loxP}$ littermates without cre. Mice were sacrificed for spine/protrusion analysis at 6 months of age. Tissue was prepared in the same manner as above, with the exception that prior to cell-filling, slices were stained with DAPI so that the dentate gyrus cell body layer could be identified. Cells were filled in the same manner as stated above, except that dentate gyrus cell body layer neurons were chosen at random. Whole cell morphological analysis was not performed, but dendritic segments of filled cells were selected for confocal imaging based on three criteria. (1) The dendritic segment had to span the 20–50 μm distance from the edge of the cell body layer. (2) The dendritic segment had to be nearly parallel to the surface of the slice, such that the entire segment could be imaged within a 6 μm thick z-stack. (3) No branching or crossing of nearby dendrites could be observed within the segment. Dendrite width, spine/protrusion density and spine/protrusion head diameter were all analyzed as stated above except that manual classification of spines/protrusions from a subset of the WT DG granule neurons provided a head diameter threshold of 0.5 μm.

Electrophysiology

Spontaneous, Miniature Synaptic Transmission in Amygdala—Coronal slices (300 um thick) including the BLA were prepared and recordings performed as described previously (Stuber et al., 2011). Briefly, 3–5 weeks after stereotaxic injections of the viral vectors (see above), mice were anesthetized with pentobarbital, perfused intracardially with 20–30 ml of modified 0°C artificial cerebrospinal fluid (aCSF) and decapitated. The brain was quickly isolated and chilled into dissecting solution. The dissecting solution contained the following (in mM): 75 sucrose, 81 NaCl, 2.5 KCl, 1.0 NaH_2PO_4, 0.1 $CaCl_2$, 4.9 $MgCl_2$, 26.2 $NaHCO_3$, and 1.5 glucose (300–305 mOsm). The bathing solution contained the following (in mM): 119 NaCl, 2.5 KCl, 1.25 NaH_2PO_4, 2.5 $CaCl_2$, 1 $MgCl_2$, 26.2 $NaHCO_3$, and 10 dextrose, saturated with 95% O2/5% CO_2. For recording of mEPSCs, the bathing solution was supplemented with Tetrodotoxin (0.5 μM) and Picrotoxin (100 μM). Slices were incubated in the bathing solution at 32°C for at least 1 h. Afterwards, slices remained at 32°C or room temperature until transferred to a submersion-type recording chamber. Whole-cell patch-clamp recordings from BLA neurons clearly identifiable as expressing YFP from the control or experimental viruses were performed using micropipettes (3–5 MΩ) made from 1.1/1.5 mm borosilicate glass (Sutter or King Precision Glass). Recording pipettes were filled with the following solution (in mM): 117 Cs-methanesulphonate, 2.8 NaCl, 5 TEA-Cl, 0.4 EGTA, 2 ATP-Mg, 0.25 GTP-Mg, 20 HEPES-CsOH (pH 7.2–7.4, 275–285 mOsm). Access resistance was frequently checked to be < 25 MΩ and stable (less than 20% of variability). Recordings were obtained using the 700B Multiclamp amplifier (Molecular Devices), and neurons were visualized using a fluorescent microscope equipped with infrared differential interference contrast. All responses were digitized at 10 kHz and filtered at 1 kHz. Data were analyzed offline using pClamp, Minianalysis (Synaptosoft) and Microsoft Excel. Student's t-test was used to evaluate significance of all analyses.

Behavior

Behaviors were done on two cohorts of mice with less stressful tests at the beginning and more stressful tests toward the end in the following order: elevated plus maze, dark/light, open field, locomotor, social interaction with a juvenile, social interaction in an open field, startle threshold, contextual and cued fear conditioning, and footshock threshold (McIlwain et al., 2001). The behavioral tests were begun at 3 weeks post virus injection. Mice were given a 24 hr inter-test interval throughout the test battery (Paylor et al., 2006). Mice were allowed 1 h to habituate to the testing room prior to beginning experiments. Significance was taken as $p < 0.05$ for all behaviors. Only mice with clear, bilateral BLA viral targeting were included in the study. (N=15 AAV-PTEN-shRNA injected mice and N=12 AAV-Luciferase-shRNA injected mice). All tests were done in accordance with IACUC and UT Southwestern Medical Center animal guidelines and protocols.

Tests of Anxiety – tests of anxiety were performed as previously reported (Tabuchi et al., 2007). For the **elevated plus maze** task mice were placed in the center of a black plexiglass elevated plus maze (each arm 33 cm in length and 5 cm wide, with 25 cm high walls on closed arms) in a dimly lit room for 5 min. 2 mazes were used and video-tracked simultaneously (Ethovision 2.3.19, Noldus; Wageningen, The Netherlands). A barrier was set between the mazes to prevent mice from seeing each other. Time spent in open and closed arms, number of open and closed entries, and time in the middle was calculated. Data were analyzed with a 1-way ANOVA. The **open field** test was performed for 10 min in a brightly lit, 48 × 48 × 48 cm white plastic arena using the Ethovision video-tracking software (Noldus). Time spent in the center zone (15 × 15 cm) and frequency to enter the center was recorded. Locomotor activity was also measured during the open field test. Data were analyzed with a 1-way ANOVA. The **dark/light** apparatus is a 2 compartment opaque plexiglass box. One side is black and kept closed and dark, while the other is white with a

fluorescent light directly above its open top. Mice were placed in the dark side for 2 min, and then the divider between the two sides was removed allowing the mouse to freely explore both chambers for 10 min. Time spent in the light and in the dark compartments was measured. Measures were taken using photobeams and MedPC software (Med Associates; St. Albans, VT). Data were analyzed with a 1-way ANOVA.

Locomotor – The locomotor test was performed as previously reported (Tabuchi et al., 2007). Mice were placed in a fresh home cage with minimal bedding for a 2 hour testing period. Lengthwise horizontal activity was monitored using photobeams linked to computer data acquisition software (San Diego Instruments, San Diego, CA). Data were analyzed with a 2-way ANOVA with repeated measures (2-way rmANOVA).

Social Interaction Tests – Tests of social interaction were performed as previously reported (Tabuchi et al., 2007). Direct **social interaction with a juvenile** took place in a novel, empty, clear, plastic mouse cage under red light as previously reported. Following a 15 min habituation in the dark, the experimental and target mice were placed in the neutral cage for two min and allowed to directly interact. Time spent interacting with the juvenile was scored by an observer blind to genotype. Social learning was assessed three days later by allowing mice to interact with the same juvenile for an additional two min. Again, time spent interacting with the juvenile was scored. Data were analyzed with a 3-way mixed ANOVA with genotype and sex as between subjects factors and test session as a within subjects factor. **Social interaction in the open field** was tested by placing experimental mice in a 48 × 48 cm^2 white plastic arena using a 6.0 × 9.5 cm porous rectangular plexiglass cage with or without an adult mouse as a target, allowing olfactory and minimal tactile interaction. Social interaction was measured as the time spent in the interaction zone (area immediately surrounding the target cage). 1-way ANOVA was used to compare time spent in the interaction zones between groups.

Startle Threshold – This task was performed exactly as described previously (Blundell et al., 2010). Briefly, mice were presented with 6 trial types of varying intensity (No Stimulus or 80, 90, 100, 110, or 120 dB pulses – eight presentations of each). Mean startle amplitudes for each condition were averaged. Data were analyzed with a 2-way rmANOVA.

Fear Conditioning – Fear conditioning was performed as described previously (Powell et al., 2004). Mice were placed in clear plexiglass shock boxes (Med Associates) for 2 min, and then two, 90 dB acoustic conditioned stimuli (CS; white noise, each 30 seconds in duration and separated by a 30 second delay) were played. Each CS co-terminated in a 2 s, 0.5 mA foot shock (US). Mice remained in the chamber for 2 min after the second pairing before returning to their home cages. Freezing behavior (motionless except respirations) was monitored at 5 s intervals by an observer blind to the genotype. To test contextual learning 24 hr later, mice were returned to the same training context and scored for freezing in the same manner. To assess cue-dependent fear conditioning, mice were placed in a novel environment with an unfamiliar vanilla odor in the afternoon following the contextual test. Freezing was measured first during a 3 min baseline period then during 3 minutes with the CS playing. Cue-dependent fear conditioning was measured by subtracting the 3 min baseline period from the 3 min CS period. Data were analyzed with a 1-way ANOVA.

Footshock Threshold – Footshock threshold analysis was performed as described previously (Blundell et al., 2009). Briefly, mice were placed in fear conditioning apparatus for a two min habituation followed by a two s footshock with an interstimulus interval of 20 s of gradually increasing intensity from 0.05 mA at 0.05 mA steps. The intensity required to elicit flinching, jumping and vocalizing was recorded by an observer blind to genotype. Data were analyzed with a 1-way ANOVA.

Results

Previous studies of Chattarji and colleagues (Govindarajan et al., 2006; Lakshminarasimhan and Chattarji, 2012) demonstrated that following chronic and acute immobilization stress, BDNF (an upstream regulator of the PI3K/AKT/mTOR pathway) and spine density concomitantly increase in the basolateral amygdala (BLA) (Lakshminarasimhan and Chattarji, 2012). Furthermore, in BDNF overexpressing transgenic mice, increased BDNF and increased neuronal spine density in BLA correlated with increased anxiety (Govindarajan et al., 2006). We initially hypothesized that increased activity of the PI3K/AKT/mTOR pathway via knockdown of PTEN would be sufficient to increase spine density in the BLA. To test this hypothesis, we injected shRNA-expressing AAV serotype 2 into the BLA that would target and knockdown PTEN transcripts preferentially in neurons (Bartlett et al., 1998). We then measured neuronal and spine/dendritic protrusion morphology and size.

Characterization of viral injections

In order to knockdown PTEN, we used AAV-PTEN-shRNA (shPTEN) injections into the BLA compared to control virus AAV-luciferase-shRNA (shLuc). Because both the shPTEN and shLuc viruses bicistronically expressed YFP, we used immunohistochemistry (IHC) against YFP to examine the accuracy of our bilateral viral injections into the BLA 3 weeks after injection (Figure 1A). We found that more than half of the injected mice showed YFP expression largely contained to the BLA bilaterally. A Paxinos plate overlayed with the localization of viral YFP expression from all the included shPTEN mice is shown in Figure 1B. Mice that did not exhibit YFP expression in the BLA, or that exhibited significant YFP expression in the central amygdala, cortex, or striatum were excluded from our studies in a manner completely blind to other results. In order to examine the anterior-posterior spread of the virus within the BLA, we again used anti-YFP antibodies to label brain sections taken every 180 μm along the anterior-posterior axis of the amygdala (Figure 1C). We found that YFP expression spread more than 1 mm along the anterior-posterior axis. Finally, we quantified the percentage of neurons expressing YFP within an infected region by co-labeling sections with anti-YFP and anti-NeuN antibodies and then calculated the percentage of NeuN+ cells that were also YFP+ (Figure 1 D–G). The percentage of neurons infected by the shPTEN and shLuc viruses was not significantly different (shPTEN, Mean – 58.80%, SEM - ±1.58%; shLuc, Mean - 54.81%, SEM - ±1.58%; $p = 0.23$, N=3 randomly chosen mice from behavioral experiments, data from 5 slices per mouse were averaged together for each of the 3 mice). While around half of the NeuN+ cells were also YFP+, it is important to note, that few of the YFP+ cells were NeuN− (Fig. 1G). Even though small numbers of other cell types may have been infected, labeling for NeuN supports what is already known about the relative neuronal tropism of AAV serotype 2 viruses (Bartlett et al., 1998).

We next tested whether the shPTEN virus effectively resulted in decreased PTEN protein levels by double-labeling YFP and PTEN in brain sections from shPTEN and shLuc injected mice. In low magnification images, shPTEN infected tissue (Figure 2A–C) revealed that PTEN protein levels were significantly decreased in regions expressing viral YFP, while shLuc infected tissue (Figure 2D–F) showed no change in PTEN levels in regions expressing viral YFP. When these sections were imaged with higher magnification, cells located within or bordering the shPTEN infected region that express detectable levels of PTEN do not express YFP (Figure 2G–I). However, in the shLuc infected cells, no detectable change in PTEN levels was observed among cells inside or outside the infected region (Figure 2J–L). Thus, shPTEN effectively reduces PTEN levels while the control virus, shLuc, does not.

To determine if PTEN function also decreased after shPTEN viral infection, we assessed the expression of phosphorylated AKT (pAKT) which is downstream of PTEN and PI3K. Under normal conditions PTEN function acts to decrease the amount of phosphatidyl-inositol trisphosphate, thereby decreasing PI3K activity and decreasing pAKT in the cell. Thus, with decreased PTEN function we expected increased pAKT within the shPTEN infected region. When we co-localized the virally expressed YFP and pAKT, low magnification images revealed that shPTEN infection dramatically increases pAKT levels (Figure 2M–O) while shLuc infected tissue does not display any increase in pAKT levels (Figure P–R). Under higher magnification we observed that cells infected with the shPTEN virus have increased pAKT levels (Figure 2S–U) while shLuc infected cells do not (Figure 2V–X). Both the PTEN and pAKT immunohistochemistry experiments were repeated in 3 pairs of mice infected with shPTEN or shLuc with representative images shown in figure 2.

PTEN knockdown in BLA neurons induces neuronal hypertrophy

In order to measure changes in the morphology of virally infected neurons, YFP+ BLA neurons were loaded with the red fluorescent dye, Alexa Fluor 568. Z-stack images of loaded cells (Figure 3A–B) were used to digitally reconstruct infected cells and analyze soma size, dendritic length and dendritic branching. Somas of shPTEN infected neurons were found to be significantly larger than in shLuc infected neurons (Figure 3C; shPTEN - mean, 4143.0 μm^3, SEM, ± 345.9 μm^3; shLuc - mean, 2636.1 μm^3, SEM, 176.3 μm^3; N=18, $p < 0.001$ using student's t-test). When we performed a Scholl analysis using concentric circles whose radii increase in increments of 30 μm, we found no change in total dendritic length (data not shown) or in the length of dendrite at any specific distance from the cell body between shPTEN and shLuc infected neurons (Figure 3D). We also did not detect any change in the total number of branch points (data not shown) or number of branch points (nodes) at any specific distance from the cell body between the two groups (Figure 3E). We did observe, however, a dramatic increase in dendrite diameter of shPTEN infected neurons that seemed to be most prominent from 30–80 μm from the cell body (Figure 3F; 2-way ANOVA, main effect of virus, $F_{(1,310)} = 35.02$, $p < 0.0001$, main effect of distance $F_{(9,310)} = 13.58$, $p < 0.0001$, virus X distance interaction $F_{(9,310)} = 0.81$, $p = 0.61$). This difference in dendrite diameter between shLuc and shPTEN infected neurons is also illustrated in Figure 4A–D. The increase in dendritic caliber and soma size are consistent with what is known about the knockdown and knockout of PTEN in the DG (Kwon et al., 2006; Kwon et al., 2003; Luikart et al., 2011; Zhou et al., 2009).

PTEN knockdown causes a decrease in thin protrusion density at distal dendritic segments and a global increase in mushroom spine size and density

Cell body and dendrite diameters were increased in the shPTEN neurons, and we wondered whether spine head diameter might also be increased. Thus, we analyzed spine heads and identified a significant increase in spine head diameter in PTEN knockdown neurons compared to shLuc-infected control neurons. Spine head diameter was measured using confocal microscopy to take high magnification, high resolution, z-stack images of dendritic segments every 10 μm up to 100 μm from the cell body (Figure 4A–D shows representative images). Overall, average spine head diameter was increased in shPTEN neurons compared to shLuc neurons at all dendritic distances measured (Figure 4E; 2-way ANOVA with repeated measures (rmANOVA), main effect of virus $F_{(1,26)} = 25.14$, $p < 0.0001$; main effect of distance $F_{(9,234)} = 2.58$, $p < 0.01$; virus X distance interaction $F_{(9,234)} = 10.54$, $p < 0.0001$).

In addition to determining the overall spine head diameter, which could be affected simply by increasing the proportion of mushroom-shaped spines compared to thin protrusions, we sub-categorized spines/protrusions into mushroom spines, and stubby spines, and thin

protrusions. After sub-categorizing spines/protrusions in this manner, we observed that mushroom spine head diameter as a separate group was increased in the shPTEN neurons (Figure 4F; main effect of virus $F_{(1,17)} = 9.14$, $p < 0.01$; main effect of distance $F_{(9,153)} = 2.19$; $p < 0.05$; virus X distance interaction $F_{(9,153)} = 1.35$, $p = 0.21$). Stubby spine and thin protrusion head diameters, however, were not different between shLuc and shPTEN neurons (Figure 4G and 4H respectively, thin protrusion "head diameters" were equated to distal neck diameters when no clear head was identified). Thus, it appears that the overall increase in spine head diameter of shPTEN neurons in the BLA can be attributed to the increase in mushroom spine head diameter in addition to possible changes in the proportion of mushroom spines.

Because knocking down PTEN has been reported by us and others to increase spine density (Kwon et al., 2006; Luikart et al., 2011; Zhou et al., 2009), we also measured spine density in shPTEN and shLuc neurons. Contrary to our own and others' previous findings using less sensitive measures, we did not find an increase in total spine density; on the contrary, statistical analysis revealed an interaction between virus and distance that suggested a *decrease* in total spine density in shPTEN neurons at the more distal segments compared to shLuc neurons with no change in density more proximally. (Figure 5A; 2-way rmANOVA, main effect of virus $F_{(1,31)} = 2.13$, $p = 0.15$; main effect of distance $F_{(9,279)} = 32.72$, $p < 0.0001$; virus X distance interaction $F_{(9,279)} = 2.02$, $p < 0.05$).

To tease apart the contribution of different spine types on spine density, we evaluated the density of mushroom spines, stubby spines and thin protrusions independently. This analysis demonstrated that mushroom spine density was *increased* in shPTEN neurons compared to shLuc neurons while both thin protrusion and stubby spine densities were *decreased* in shPTEN neurons compared to shLuc neurons (Figure 5B–D; mushroom, main effect of virus $F_{(1,31)} = 10.96$, $p < 0.01$; main effect of distance $F_{(9,279)} = 19.70$, $p < 0.0001$; virus X distance interaction $F_{(9,279)} = 1.02$, $p = 0.42$; thin, main effect of virus $F_{(1,31)} = 5.12$, $p < 0.05$; main effect of distance $F_{(9,279)} = 25.62$, $p < 0.0001$; virus X distance interaction $F_{(9,279)} = 2.07$, $p < 0.05$; stubby, main effect of virus $F_{(1,31)} = 14.99$, $p < 0.001$; main effect of distance $F_{(9,279)} = 2.97$, $p < 0.01$; virus X distance interaction $F_{(9,279)} = 0.61$, $p = 0.79$). These differential changes in spine/protrusion subtypes result in shPTEN neurons with a dramatically increased mushroom spine fraction along the entire length of the dendrite compared to shLuc neurons (Figure 5E; main effect of virus $F_{(1,26)} = 34.44$, $p < 0.0001$, main effect of distance $F_{(9,234)} = 2.65$, $p < 0.01$; virus X distance interaction $F_{(9,234)} = 9.90$, $p < 0.0001$). When the mushroom spine fraction was calculated for the entire 100 μm length of dendrite, 39.2% (SEM ± 3.02%) of spines in shPTEN neurons were mushroom spines, while only 22.95% (SEM ± 2.64%) of spines were mushroom spines in shLuc neurons (Figure 5F; student's t-test, $p < 0.001$).

PTEN knockdown-induced shift from thin protrusions to mushroom spines is not specific to amygdala neurons

Our findings in basolateral amygdala neurons of decreased spine density at distal segments and a shift from thin protrusions to mushroom spines directly contrasted with our own previous reports of increased spine density in dentate gyrus granule neurons of PTEN conditional knockout mice. These findings could be explained by regional and neuronal differences or by an increased sensitivity of Alexa Fluor 568 cell filling followed by confocal spine-imaging compared to previously used methods. In an effort to distinguish between these interpretations, we used the same fluorescent cell filling, imaging, and spine analysis techniques on dentate gyrus granule neurons in PTEN conditional knockout mice (PTEN cKO) as we used in the BLA. We purposely used PTEN cKO mice rather than PTEN shRNA viral infection in dentate gyrus so that we could directly compare our results with

fluorescent imaging to our previous results from Golgi staining methods used in our prior publications (Kwon et al., 2006; Zhou et al., 2009). Similar to previous work in these PTEN cKO mice, images were taken of dentate gyrus granule neuron dendrites spanning the 20–50 μm distance from the dentate gyrus cell body layer (representative images in Figure 6A–B). As expected, and similar to our findings in the BLA and previous reports (Luikart et al., 2011; Zhou et al., 2009), we found that PTEN cKO neurons had increased dendritic diameter (Figure 6C; WT, 0.80 ± 0.04 μm; PTEN cKO, 1.85 ± 0.13 μm, student's t-test $p < 0.0001$). We also found that, similar to the BLA shPTEN neurons, spine head diameter was increased; in the DG, however, a significant increase in spine head diameter was observed across all three spine types including thin protrusions (Figure 6D; All spines, WT 0.38 ± 0.01 μm, PTEN cKO 0.63 ± 0.02 μm, $p < 0.0001$; mushroom spines, WT 0.77 ± 0.02 μm, PTEN cKO 0.95 ± 0.02 μm, $p < 0.0001$; thin protrusions, WT 0.32 ± 0.006 μm, PTEN cKO 0.37 ± 0.006 μm, $p < 0.05$; stubby spines, WT 0.40 ± 0.04 μm, PTEN cKO 0.70 ± 0.04 μm, $p < 0.0001$).

As spine density was previously reported to be increased in dentate gyrus granule neurons of PTEN cKO mice (Kwon et al., 2006), we expected similar results. However, we found that similar to the shPTEN neurons in BLA, there was an increase in mushroom spine density with a corresponding decrease in thin protrusion density and a small increase in stubby spine density that resulted in no change in overall spine/protrusion density (Figure 6E; all spines, WT 3.93 ± 0.27 spines/μm, PTEN cKO 3.87 ± 0.33 spines/μm, $p = 0.89$; mushroom spines, WT 0.48 ± 0.04 spines/μm, PTEN cKO 1.67 ± 0.17 spines/μm, $p < 0.0001$; thin protrusions, WT 3.36 ± 0.27 spines/μm, PTEN cKO 2.02 ± 0.19 spines/μm, $p < 0.001$; stubby, WT 0.09 ± 0.02 spines/μm, PTEN cKO 0.18 ± 0.02 spines/μm, $p < 0.01$). Finally, again similar to shPTEN neurons in BLA, the mushroom spine fraction (# mushroom spines/# total spines) in the PTEN cKO dentate granule neurons was significantly and dramatically increased compared to WT neurons (Figure 6F; WT 12.9.0 ± 1.2%, PTEN cKO 42.3 ± 3.2%, $p < 0.0001$). Thus, PTEN deficiency-induced increases in mushroom spine density and corresponding decreases in thin protrusion density are common to both amygdala neurons and dentate granule neurons, even using different knockdown approaches and different durations of knockdowns. These results suggest a widespread role for the PTEN/PI3K/AKT/mTOR pathway in maintaining the proper balance of thin and mushroom spines in neurons in both brain regions.

shPTEN infected neurons display increased miniature EPSC neurotransmission

Dendritic spines are a major site for excitatory synaptic neurotransmission (Bourne and Harris 2007). Spines of diverse sizes and morphologies are thought to represent different stages of spine maturity and to vary in function (Bourne and Harris, 2007; Matsuo et al., 2008). As demonstrated above, shPTEN infected neurons had increased mushroom spine density, decreased thin protrusion density at distal segments, and increased spine head diameter. The differences in these dendritic spine parameters suggest that synaptic transmission may also be altered due to knockdown of PTEN. As an initial step in investigating this possibility, we recorded miniature excitatory post-synaptic currents (mEPSC) from the BLA in coronal brain slices 3–5 weeks after vector injection. shPTEN or shLuc infected neurons expressing YFP were detected by epifluorescence. We found that shPTEN infected neurons showed a significant increase in mEPSC frequency (Figure 7A and B; WT 1.18 ± 0.40 Hz, PTEN cKO 3.66 ± 1.01 Hz, $p < 0.030$). The amplitude of mEPSC was also increased (Figure 7C and D; WT 17.39 ± 1.03 Hz, PTEN cKO 23.22 ± 2.6Hz, $p < 0.046$). Similar functional results have been published for dentate granule neurons with decreased PTEN (Luikart et al., 2011), supporting a conclusion of altered synaptic function due to PTEN knockdown.

Lack of associated behavioral abnormalities following PTEN knockdown in a subset of BLA neurons

Given previously published findings correlating increased BNDF expression and increased functional spine density in the BLA with increased anxiety-like behaviors (Govindarajan et al., 2006), we sought to determine if decreased PTEN expression and resulting increased PI3K/AKT/mTOR signaling would also correlate with increased anxiety-related behavior. In spite of a reduction in PTEN as demonstrated by immunohistochemistry and alterations in the number of functional, mature synaptic spines in the BLA, we observed no alterations in anxiety-related tasks including elevated plus maze, open field and dark/light box (Figure 8A–C). Similarly, no alterations in other behavioral tasks were observed including social interaction with a juvenile, fear conditioning, startle threshold, social interaction in an open field, and locomotor activity (Figure 8D–H).

Discussion

Previous work by our lab and others reported that loss of PTEN from DG granule neurons causes neuronal hypertrophy and increased spine density (Kwon et al., 2006; Kwon et al., 2001; Luikart et al., 2011). Loss of PTEN induces upregulation of pAKT and its downstream targets including mTOR. Inhibiting mTOR reversed the neuronal and synaptic effects of PTEN deletion in DG granule neurons (Kwon et al., 2003; Zhou et al., 2009). Additionally, PTEN knockdown increases mEPSC frequency and amplitude in dentate gyrus granule neurons (Luikart et al., 2011). In accordance with these reports, we found neuronal hypertrophy in BLA neurons after virally-mediated PTEN knockdown, measured as increased soma size and dendritic caliber (Figure 3C and F). Thus, many of our findings support and extend previous work on PTEN in the brain. Moreover, we extended previous findings to include increased diameter of mushroom spine heads (Figure 4F–G).

In contrast to previous reports, however, our data suggest that PTEN knockdown in neurons does not increase total spine/protrusion density, but instead induces a shift in the mushroom:thin ratio such that the density of mushroom spines are increased while thin protrusion density is decreased in distal dendritic segments (Figure 5). In our analysis of spine morphology, we are unable to distinguish between thin spines and filopodia, leaving room to question whether one or both of those categories of protrusions is decreasing after PTEN knockdown. Nevertheless, our findings are strengthened by similar results in a second brain region using cre recombination for PTEN knockdown and imaging spines in older mice (6 months old). In addition, our results following relatively acute viral knockdown in the BLA and those following chronic knockout of PTEN in the dentate gyrus demonstrate similar effects.

Interestingly, we still observed an increase in spontaneous synaptic activity in shPTEN infected BLA neurons in spite of a decrease in total spine density at more distal segments (Figure 7). The increased mEPSC frequency is most parsimoniously explained by increased density of mushroom spines, thought to represent more mature/active synapses (Bourne and Harris, 2007), relative to thin protrusion density. Of course, mEPSC recordings favor synapses that are electronically closer to the soma. Our data suggest that upregulation of the PI3K/AKT/mTOR pathway does not increase spine/protrusion density, but instead increases the fraction of more mature, functional synapses in the BLA.

Since most studies examining the effects of PTEN knockdown on spine density were done in dentate gyrus (Kwon et al., 2006; Kwon et al., 2001; Luikart et al., 2011), one explanation for our novel findings in the BLA could be that DG and BLA respond differently to PTEN knockdown. However, our findings were similar in both brain regions. Alternatively, our results could be explained by a difference in spine imaging technique. Previous studies used

Golgi staining and light microscopy (Govindarajan et al., 2006; Kwon et al., 2006) or confocal imaging of virally expressed GFP (Luikart et al., 2011). Virally expressed GFP may not be concentrated enough in small spines for their detection, or there may be significant background signal due to many cells expressing GFP. In addition, imaging spines after Golgi staining prevents the observation of spines in front of or behind the dendrite, yielding an apparently lower total spine density. Cell filling, however, may allow for an improved, 3-dimensional resolution due to a high intensity of fluorescent dye in spines and throughout the dendrites while producing little to no background from surrounding tissue or cells. We postulate that these differences in resolution resulted in better detection of thin protrusions and smaller spines in our study as a result of more efficient spread of fluorescent dyes into even the thinnest dendritic protrusions. Another potential explanation for our different findings may simply be differences in fixation techniques and artifacts that could have been induced by our methods. Such artifactual differences, of course, would have to be differentially affected by the status of PTEN knockdown since we see clear, significant differences between control and experimental conditions in spine density.

To examine these alternative explanations for our novel findings, we measured spine density in DG granule neurons in PTEN cKO mice using the cell-fill approach. PTEN knockdown in DG decreased thin protrusion density and increased mushroom spine density without changing total spine density (Figure 6E–F). The similar results in the DG and BLA using two different approaches for knocking down PTEN, along with increased overall spine density counts using our technique compared to previous reports (Kwon et al., 2006; Luikart et al., 2011; Zhou et al., 2009), supports the hypothesis that cell filling techniques allow for better visualization of small spines and more accurate measurement of PTEN's effects on spine density/function. Overall, these data imply that loss of PTEN has similar effects on spine density and morphology in the DG and BLA neurons, and that in order to observe this shift from thin protrusions to mushroom spines one must be able to image the smaller thin protrusions which may be missed with other techniques. It is of additional interest that both chronic PTEN deletion in DG and more acute PTEN knockdown in BLA led to qualitatively similar results.

Similar to studies in the hippocampus (Luikart et al., 2011), we demonstrate that knockdown of PTEN in BLA causes an increase in the frequency and amplitude of mEPSCs. As pointed out above, although we saw no indication suggesting an increase in the total number of synapses after PTEN knockdown, there was an important increase in the relative number and size of mushroom spines all along the dendritic arborization. Mushroom spines are thought to be more active than thin protrusions (Fiala et al., 2002). Interestingly, spine head volume correlates with the size of the presynaptic readily releasable pool and with the number of docked-vesicles (Dobrunz and Stevens, 1997; Harris and Stevens, 1989), which could affect the frequency of mEPSCs due to presynaptic changes. Furthermore, the size of dendritic spines is also correlated with the area of the postsynaptic density and the number of glutamatergic receptors at the synapse (Arellano et al., 2007; Harris and Stevens, 1989; Nusser et al., 1998). This is consistent with the increase in mEPSC amplitude shown here after knockdown of PTEN. Increased mEPSC amplitude is also consistent with a similar outcome due to an increase in surface expression of AMPA receptors after leptin-induced PTEN inhibition (Moult et al., 2010). Thus, the increase in frequency and amplitude in mEPSC observed after knockdown of PTEN in BLA are correlated with an increase in the number and diameter, of the “more mature” mushroom-type of synapse.

Because the amygdala is part of the circuitry known to regulate fear and anxiety (Davis et al., 1994; Johnson et al., 2008; LeDoux, 2007), we predicted that knockdown on PTEN and corresponding increases in synaptic spine size and function would alter related behaviors in our model. Despite BLA neuronal hypertrophy, shifting of spine subtypes, and increased

mEPSC frequency and amplitude in neurons lacking PTEN-expression in the BLA, these changes had no effect on multiple amygdala-dependent behaviors. While these negative behavioral data are important to report, they do not exclude a role for PTEN in the BLA in any of the behavioral tasks reported due to the virus only targeting 60% of BLA neurons within infected regions. Indeed, PTEN and other factors downstream of BDNF may still be responsible for the increased anxiety-related behaviors observed in BDNF overexpressing mice (Govindarajan et al., 2006). Alternative techniques of manipulating PTEN in the BLA may shed further light on the role of PTEN in behavior.

PTEN mutations have been implicated in human autism (Boccone et al., 2006; Butler et al., 2005; Buxbaum et al., 2007; Goffin et al., 2001; Herman et al., 2007; McBride et al., 2010; Orrico et al., 2009; Stein et al., 2010; Varga et al., 2009; Zori et al., 1998), and PTEN conditional knockout limited to the cortex and hippocampus results in alterations in social interaction, an effect that can be reversed by mTOR inhibition (Kwon et al., 2006; Zhou et al., 2009). In the present study, we assessed whether PTEN knockdown isolated to the BLA could result in social behavior abnormalities. Interestingly, we found no alterations in locomotor activity, social interaction with a juvenile, social interaction in an open field, startle threshold, fear conditioning, or footshock threshold in mice treated with shPTEN in the bilateral BLA. These findings support the conclusion that the social and anxiety phenotypes observed in the PTEN conditional KO mice (Kwon et al., 2006; Zhou et al., 2009) are subserved largely by loss of PTEN in hippocampus or cortex, the brain regions in which PTEN was conditionally deleted in this model. As noted, however, the present study does not completely rule out a role for PTEN in the BLA in any of the behaviors examined due to only a fraction of BLA neurons being affected.

In summary, our findings support a novel role for PTEN in modulation of spine morphology. Our data suggest that the mechanism leading to increased synaptic activity after PTEN knockdown may not be increased total spine density. Instead, our data implicate the PTEN/PI3K/AKT/mTOR pathway as an inducer of synaptic maturation by shifting the mushroom:thin ratio in favor of mushroom spines without dramatically altering total spine/protrusion density. It seems most likely that loss of PTEN results in conversion of thin protrusions into mature, functional mushroom spines. We cannot rule out, however, that this shift is occurring via *de novo* mushroom spine formation with concurrent pruning of the thin protrusion population. Given the disease processes for which the PTEN/AKT/mTOR pathway has been implicated, including autism (Butler et al., 2005; Buxbaum et al., 2007), understanding the role of this pathway in neuronal and synaptic growth and maturation is vital to understanding the pathophysiology of these disorders.

Acknowledgments

This work was supported by National Institute of Mental Health MH081164 (CMP), National Institute of Child Health and Human Development HD069560 (CMP), Autism Speaks (CMP), Lowe Foundation (CMP), Crystal Charity Ball (CMP), and The Hartwell Foundation (CMP).

Other Acknowledgements

We thank Dr. Patrick Hoff, Dr. John Morisson and Dr. Dani Dumitriu at Mount Sinai for training in the techniques used for neuronal cell fills and analysis using NeuronStudio Software. Dr. Michael Cherry and Nathan A. Haws helped with statistical analysis.

Role of Authors

All authors had full access to all the data in the study and take responsibility for the integrity of the data and the accuracy of the data analysis. M.E.H. & C.M.P. conceived and designed the experiments; M.E.H, T.J., F.E-B., A.W., G.D.S., D.R.S., G.S., carried them out with input from C.M.P., M.K., S.R., & A.B.; M.E.H., F.E-B., G.D.S. & C.M.P. performed statistical analysis; and M.E.H wrote the paper with input from all authors.

References

Abel TW, Baker SJ, Fraser MM, Tihan T, Nelson JS, Yachnis AT, Bouffard JP, Mena H, Burger PC, Eberhart CG. Lhermitte-Duclos disease: a report of 31 cases with immunohistochemical analysis of the PTEN/AKT/mTOR pathway. Journal of neuropathology and experimental neurology. 2005; 64(4):341–349. [PubMed: 15835270]

Arellano JI, Benavides-Piccione R, Defelipe J, Yuste R. Ultrastructure of dendritic spines: correlation between synaptic and spine morphologies. Frontiers in neuroscience. 2007; 1(1):131–143. [PubMed: 18982124]

Backman SA, Stambolic V, Suzuki A, Haight J, Elia A, Pretorius J, Tsao MS, Shannon P, Bolon B, Ivy GO, Mak TW. Deletion of Pten in mouse brain causes seizures, ataxia and defects in soma size resembling Lhermitte-Duclos disease. Nat Genet. 2001; 29(4):396–403. [PubMed: 11726926]

Bartlett JS, Samulski RJ, McCown TJ. Selective and rapid uptake of adeno-associated virus type 2 in brain. Hum Gene Ther. 1998; 9(8):1181–1186. [PubMed: 9625257]

Besson A, Robbins SM, Yong VW. PTEN/MMAC1/TEP1 in signal transduction and tumorigenesis. Eur J Biochem. 1999; 263(3):605–611. [PubMed: 10469123]

Blundell J, Kaeser PS, Sudhof TC, Powell CM. RIM1alpha and interacting proteins involved in presynaptic plasticity mediate prepulse inhibition and additional behaviors linked to schizophrenia. The Journal of neuroscience : the official journal of the Society for Neuroscience. 2010; 30(15): 5326–5333. [PubMed: 20392954]

Blundell J, Tabuchi K, Bolliger MF, Blaiss CA, Brose N, Liu X, Sudhof TC, Powell CM. Increased anxiety-like behavior in mice lacking the inhibitory synapse cell adhesion molecule neuroligin 2. Genes Brain Behav. 2009; 8(1):114–126. [PubMed: 19016888]

Boccone L, Dessi V, Zappu A, Piga S, Piludu MB, Rais M, Massidda C, De Virgiliis S, Cao A, Loudianos G. Bannayan-Riley-Ruvalcaba syndrome with reactive nodular lymphoid hyperplasia and autism and a PTEN mutation. American journal of medical genetics. 2006; 140(18):1965–1969. [PubMed: 16894538]

Bourne J, Harris KM. Do thin spines learn to be mushroom spines that remember? Curr Opin Neurobiol. 2007; 17(3):381–386. [PubMed: 17498943]

Butler MG, Dasouki MJ, Zhou XP, Talebizadeh Z, Brown M, Takahashi TN, Miles JH, Wang CH, Stratton R, Pilarski R, Eng C. Subset of individuals with autism spectrum disorders and extreme macrocephaly associated with germline PTEN tumour suppressor gene mutations. J Med Genet. 2005; 42(4):318–321. [PubMed: 15805158]

Buxbaum JD, Cai G, Chaste P, Nygren G, Goldsmith J, Reichert J, Anckarsater H, Rastam M, Smith CJ, Silverman JM, Hollander E, Leboyer M, Gillberg C, Verloes A, Betancur C. Mutation screening of the PTEN gene in patients with autism spectrum disorders and macrocephaly. Am J Med Genet B Neuropsychiatr Genet. 2007; 144B(4):484–491. [PubMed: 17427195]

Dahia PL. PTEN, a unique tumor suppressor gene. Endocr Relat Cancer. 2000; 7(2):115–129. [PubMed: 10903528]

Davis M, Rainnie D, Cassell M. Neurotransmission in the rat amygdala related to fear and anxiety. Trends in neurosciences. 1994; 17(5):208–214. [PubMed: 7520203]

Di Cristofano A, Pandolfi PP. The multiple roles of PTEN in tumor suppression. Cell. 2000; 100(4): 387–390. [PubMed: 10693755]

Dobrunz LE, Stevens CF. Heterogeneity of release probability, facilitation, and depletion at central synapses. Neuron. 1997; 18(6):995–1008. [PubMed: 9208866]

Downes CP, Bennett D, McConnachie G, Leslie NR, Pass I, MacPhee C, Patel L, Gray A. Antagonism of PI 3-kinase-dependent signalling pathways by the tumour suppressor protein, PTEN. Biochem Soc Trans. 2001; 29(Pt 6):846–851. [PubMed: 11709086]

Dumitriu D, Berger SI, Hamo C, Hara Y, Bailey M, Hamo A, Grossman YS, Janssen WG, Morrison JH. Vamping: stereology-based automated quantification of fluorescent puncta size and density. J Neurosci Methods. 2012a; 209(1):97–105. [PubMed: 22683698]

Dumitriu D, Hao J, Hara Y, Kaufmann J, Janssen WG, Lou W, Rapp PR, Morrison JH. Selective changes in thin spine density and morphology in monkey prefrontal cortex correlate with aging-

related cognitive impairment. The Journal of neuroscience : the official journal of the Society for Neuroscience. 2010; 30(22):7507–7515. [PubMed: 20519525]

Dumitriu D, Laplant Q, Grossman YS, Dias C, Janssen WG, Russo SJ, Morrison JH, Nestler EJ. Subregional, dendritic compartment, and spine subtype specificity in cocaine regulation of dendritic spines in the nucleus accumbens. The Journal of neuroscience : the official journal of the Society for Neuroscience. 2012b; 32(20):6957–6966. [PubMed: 22593064]

Dumitriu D, Rodriguez A, Morrison JH. High-throughput, detailed, cell-specific neuroanatomy of dendritic spines using microinjection and confocal microscopy. Nat Protoc. 2011; 6(9):1391–1411. [PubMed: 21886104]

Encinas JM, Vaahtokari A, Enikolopov G. Fluoxetine targets early progenitor cells in the adult brain. Proc Natl Acad Sci USA. 2006; 103(21):8233–8238. [PubMed: 16702546]

Eng C. The role of PTEN, a phosphatase gene, in inherited and sporadic nonmedullary thyroid tumors. Recent Prog Horm Res. 1999; 54:441–452. discussion 453. [PubMed: 10548886]

Eng C. PTEN: one gene, many syndromes. Hum Mutat. 2003; 22(3):183–198. [PubMed: 12938083]

Fiala JC, Allwardt B, Harris KM. Dendritic spines do not split during hippocampal LTP or maturation. Nature neuroscience. 2002; 5(4):297–298.

Forster MD, Dedes KJ, Sandhu S, Frentzas S, Kristeleit R, Ashworth A, Poole CJ, Weigelt B, Kaye SB, Molife LR. Treatment with olaparib in a patient with PTEN-deficient endometrioid endometrial cancer. Nat Rev Clin Oncol. 2011; 8(5):302–306. [PubMed: 21468130]

Fraser MM, Bayazitov IT, Zakharenko SS, Baker SJ. Phosphatase and tensin homolog, deleted on chromosome 10 deficiency in brain causes defects in synaptic structure, transmission and plasticity, and myelination abnormalities. Neuroscience. 2008; 151(2):476–488. [PubMed: 18082964]

Goffin A, Hoefsloot LH, Bosgoed E, Swillen A, Fryns JP. PTEN mutation in a family with Cowden syndrome and autism. Am J Med Genet. 2001; 105(6):521–524. [PubMed: 11496368]

Govindarajan A, Rao BS, Nair D, Trinh M, Mawjee N, Tonegawa S, Chattarji S. Transgenic brain-derived neurotrophic factor expression causes both anxiogenic and antidepressant effects. Proc Natl Acad Sci USA. 2006; 103(35):13208–13213. [PubMed: 16924103]

Hao J, Rapp PR, Leffler AE, Leffler SR, Janssen WG, Lou W, McKay H, Roberts JA, Wearne SL, Hof PR, Morrison JH. Estrogen alters spine number and morphology in prefrontal cortex of aged female rhesus monkeys. The Journal of neuroscience : the official journal of the Society for Neuroscience. 2006; 26(9):2571–2578. [PubMed: 16510735]

Harris KM, Stevens JK. Dendritic spines of CA 1 pyramidal cells in the rat hippocampus: serial electron microscopy with reference to their biophysical characteristics. The Journal of neuroscience : the official journal of the Society for Neuroscience. 1989; 9(8):2982–2997. [PubMed: 2769375]

Herman GE, Butter E, Enrile B, Pastore M, Prior TW, Sommer A. Increasing knowledge of PTEN germline mutations: Two additional patients with autism and macrocephaly. American journal of medical genetics. 2007; 143(6):589–593. [PubMed: 17286265]

Hobert JA, Eng C. PTEN hamartoma tumor syndrome: an overview. Genet Med. 2009; 11(10):687–694. [PubMed: 19668082]

Hoeffer CA, Klann E. mTOR signaling: at the crossroads of plasticity, memory and disease. Trends in neurosciences. 2010; 33(2):67–75. [PubMed: 19963289]

Johnson LR, Hou M, Ponce-Alvarez A, Gribelyuk LM, Alphs HH, Albert L, Brown BL, Ledoux JE, Doyere V. A recurrent network in the lateral amygdala: a mechanism for coincidence detection. Frontiers in neural circuits. 2008; 2:3. [PubMed: 19104668]

Kwon CH, Luikart BW, Powell CM, Zhou J, Matheny SA, Zhang W, Li Y, Baker SJ, Parada LF. Pten regulates neuronal arborization and social interaction in mice. Neuron. 2006; 50(3):377–388. [PubMed: 16675393]

Kwon CH, Zhu X, Zhang J, Baker SJ. mTor is required for hypertrophy of Pten-deficient neuronal soma in vivo. Proc Natl Acad Sci USA. 2003; 100(22):12923–12928. [PubMed: 14534328]

Kwon CH, Zhu X, Zhang J, Knoop LL, Tharp R, Smeyne RJ, Eberhart CG, Burger PC, Baker SJ. Pten regulates neuronal soma size: a mouse model of Lhermitte-Duclos disease. Nat Genet. 2001; 29(4):404–411. [PubMed: 11726927]

Lakshminarasimhan H, Chattarji S. Stress leads to contrasting effects on the levels of brain derived neurotrophic factor in the hippocampus and amygdala. PloS one. 2012; 7(1):e30481. [PubMed: 22272355]

LeDoux J. The amygdala. Current biology : CB. 2007; 17(20):R868–874. [PubMed: 17956742]

Leslie NR, Downes CP. PTEN: The down side of PI 3-kinase signalling. Cell Signal. 2002; 14(4):285–295. [PubMed: 11858936]

Li J, Yen C, Liaw D, Podsypanina K, Bose S, Wang SI, Puc J, Miliaresis C, Rodgers L, McCombie R, Bigner SH, Giovanella BC, Ittmann M, Tycko B, Hibshoosh H, Wigler MH, Parsons R. PTEN, a putative protein tyrosine phosphatase gene mutated in human brain, breast, and prostate cancer. Science. 1997; 275(5308):1943–1947. [PubMed: 9072974]

Luikart BW, Schnell E, Washburn EK, Bensen AL, Tovar KR, Westbrook GL. Pten knockdown in vivo increases excitatory drive onto dentate granule cells. The Journal of neuroscience : the official journal of the Society for Neuroscience. 2011; 31(11):4345–4354. [PubMed: 21411674]

Maehama T, Dixon JE. The tumor suppressor, PTEN/MMAC1, dephosphorylates the lipid second messenger, phosphatidylinositol 3,4,5-trisphosphate. The Journal of biological chemistry. 1998; 273(22):13375–13378. [PubMed: 9593664]

Maehama T, Dixon JE. PTEN: a tumour suppressor that functions as a phospholipid phosphatase. Trends Cell Biol. 1999; 9(4):125–128. [PubMed: 10203785]

Matsuo N, Reijmers L, Mayford M. Spine-type-specific recruitment of newly synthesized AMPA receptors with learning. Science. 2008; 319(5866):1104–1107. [PubMed: 18292343]

McBride KL, Varga EA, Pastore MT, Prior TW, Manickam K, Atkin JF, Herman GE. Confirmation study of PTEN mutations among individuals with autism or developmental delays/mental retardation and macrocephaly. Autism Res. 2010; 3(3):137–141. [PubMed: 20533527]

McDonald AJ. Neurons of the lateral and basolateral amygdaloid nuclei: a Golgi study in the rat. J Comp Neurol. 1982; 212(3):293–312. [PubMed: 6185547]

McIlwain KL, Merriweather MY, Yuva-Paylor LA, Paylor R. The use of behavioral test batteries: effects of training history. Physiol Behav. 2001; 73(5):705–717. [PubMed: 11566205]

Moldrich RX, Gobius I, Pollak T, Zhang J, Ren T, Brown L, Mori S, De Juan Romero C, Britanova O, Tarabykin V, Richards LJ. Molecular regulation of the developing commissural plate. J Comp Neurol. 2010; 518(18):3645–3661. [PubMed: 20653027]

Moult PR, Cross A, Santos SD, Carvalho AL, Lindsay Y, Connolly CN, Irving AJ, Leslie NR, Harvey J. Leptin regulates AMPA receptor trafficking via PTEN inhibition. The Journal of neuroscience : the official journal of the Society for Neuroscience. 2010; 30(11):4088–4101. [PubMed: 20237279]

Mullen RJ, Buck CR, Smith AM. NeuN, a neuronal specific nuclear protein in vertebrates. Development. 1992; 116(1):201–211. [PubMed: 1483388]

Nelen MR, van Staveren WC, Peeters EA, Hassel MB, Gorlin RJ, Hamm H, Lindboe CF, Fryns JP, Sijmons RH, Woods DG, Mariman EC, Padberg GW, Kremer H. Germline mutations in the PTEN/MMAC1 gene in patients with Cowden disease. Hum Mol Genet. 1997; 6(8):1383–1387. [PubMed: 9259288]

Nusser Z, Lujan R, Laube G, Roberts JD, Molnar E, Somogyi P. Cell type and pathway dependence of synaptic AMPA receptor number and variability in the hippocampus. Neuron. 1998; 21(3):545–559. [PubMed: 9768841]

Orloff MS, Eng C. Genetic and phenotypic heterogeneity in the PTEN hamartoma tumour syndrome. Oncogene. 2008; 27(41):5387–5397. [PubMed: 18794875]

Orrico A, Galli L, Buoni S, Orsi A, Vonella G, Sorrentino V. Novel PTEN mutations in neurodevelopmental disorders and macrocephaly. Clin Genet. 2009; 75(2):195–198. [PubMed: 18759867]

Paylor R, Spencer CM, Yuva-Paylor LA, Pieke-Dahl S. The use of behavioral test batteries, II: effect of test interval. Physiol Behav. 2006; 87(1):95–102. [PubMed: 16197969]

Powell CM, Schoch S, Monteggia L, Barrot M, Matos MF, Feldmann N, Sudhof TC, Nestler EJ. The presynaptic active zone protein RIM1alpha is critical for normal learning and memory. Neuron. 2004; 42(1):143–153. [PubMed: 15066271]

Pun RY, Rolle IJ, Lasarge CL, Hosford BE, Rosen JM, Uhl JD, Schmeltzer SN, Faulkner C, Bronson SL, Murphy BL, Richards DA, Holland KD, Danzer SC. Excessive activation of mTOR in postnatally generated granule cells is sufficient to cause epilepsy. Neuron. 2012; 75(6):1022–1034. [PubMed: 22998871]

Rodriguez A, Ehlenberger DB, Dickstein DL, Hof PR, Wearne SL. Automated three-dimensional detection and shape classification of dendritic spines from fluorescence microscopy images. PloS one. 2008; 3(4):e1997. [PubMed: 18431482]

Rodriguez A, Ehlenberger DB, Hof PR, Wearne SL. Rayburst sampling, an algorithm for automated three-dimensional shape analysis from laser scanning microscopy images. Nat Protoc. 2006; 1(4): 2152–2161. [PubMed: 17487207]

Steck PA, Pershouse MA, Jasser SA, Yung WK, Lin H, Ligon AH, Langford LA, Baumgard ML, Hattier T, Davis T, Frye C, Hu R, Swedlund B, Teng DH, Tavtigian SV. Identification of a candidate tumour suppressor gene, MMAC1, at chromosome 10q23.3 that is mutated in multiple advanced cancers. Nat Genet. 1997; 15(4):356–362. [PubMed: 9090379]

Stein MT, Elias ER, Saenz M, Pickler L, Reynolds A. Autistic spectrum disorder in a 9-year-old girl with macrocephaly. J Dev Behav Pediatr. 2010; 31(7):632–634. [PubMed: 20814261]

Stuber GD, Sparta DR, Stamatakis AM, van Leeuwen WA, Hardjoprajitno JE, Cho S, Tye KM, Kempadoo KA, Zhang F, Deisseroth K, Bonci A. Excitatory transmission from the amygdala to nucleus accumbens facilitates reward seeking. Nature. 2011; 475(7356):377–380. [PubMed: 21716290]

Suzuki A, Yamaguchi MT, Ohteki T, Sasaki T, Kaisho T, Kimura Y, Yoshida R, Wakeham A, Higuchi T, Fukumoto M, Tsubata T, Ohashi PS, Koyasu S, Penninger JM, Nakano T, Mak TW. T cell-specific loss of Pten leads to defects in central and peripheral tolerance. Immunity. 2001; 14(5):523–534. [PubMed: 11371355]

Tabuchi K, Blundell J, Etherton MR, Hammer RE, Liu X, Powell CM, Sudhof TC. A neuroligin-3 mutation implicated in autism increases inhibitory synaptic transmission in mice. Science. 2007; 318(5847):71–76. [PubMed: 17823315]

Varga EA, Pastore M, Prior T, Herman GE, McBride KL. The prevalence of PTEN mutations in a clinical pediatric cohort with autism spectrum disorders, developmental delay, and macrocephaly. Genet Med. 2009; 11(2):111–117. [PubMed: 19265751]

Vazquez F, Sellers WR. The PTEN tumor suppressor protein: an antagonist of phosphoinositide 3-kinase signaling. Biochim Biophys Acta. 2000; 1470(1):M21–35. [PubMed: 10656987]

Waite KA, Eng C. Protean PTEN: form and function. Am J Hum Genet. 2002; 70(4):829–844. [PubMed: 11875759]

Wearne SL, Rodriguez A, Ehlenberger DB, Rocher AB, Henderson SC, Hof PR. New techniques for imaging, digitization and analysis of three-dimensional neural morphology on multiple scales. Neuroscience. 2005; 136(3):661–680. [PubMed: 16344143]

Xiong Q, Oviedo HV, Trotman LC, Zador AM. PTEN Regulation of Local and Long-Range Connections in Mouse Auditory Cortex. The Journal of neuroscience : the official journal of the Society for Neuroscience. 2012; 32(5):1643–1652. [PubMed: 22302806]

Zhang XC, Piccini A, Myers MP, Van Aelst L, Tonks NK. Functional analysis of the protein phosphatase activity of PTEN. Biochem J. 2012; 444(3):457–464. [PubMed: 22413754]

Zhou J, Blundell J, Ogawa S, Kwon CH, Zhang W, Sinton C, Powell CM, Parada LF. Pharmacological inhibition of mTORC1 suppresses anatomical, cellular, and behavioral abnormalities in neural-specific Pten knock-out mice. The Journal of neuroscience : the official journal of the Society for Neuroscience. 2009; 29(6):1773–1783. [PubMed: 19211884]

Zori RT, Marsh DJ, Graham GE, Marliss EB, Eng C. Germline PTEN mutation in a family with Cowden syndrome and Bannayan-Riley-Ruvalcaba syndrome. Am J Med Genet. 1998; 80(4):399–402. [PubMed: 9856571]

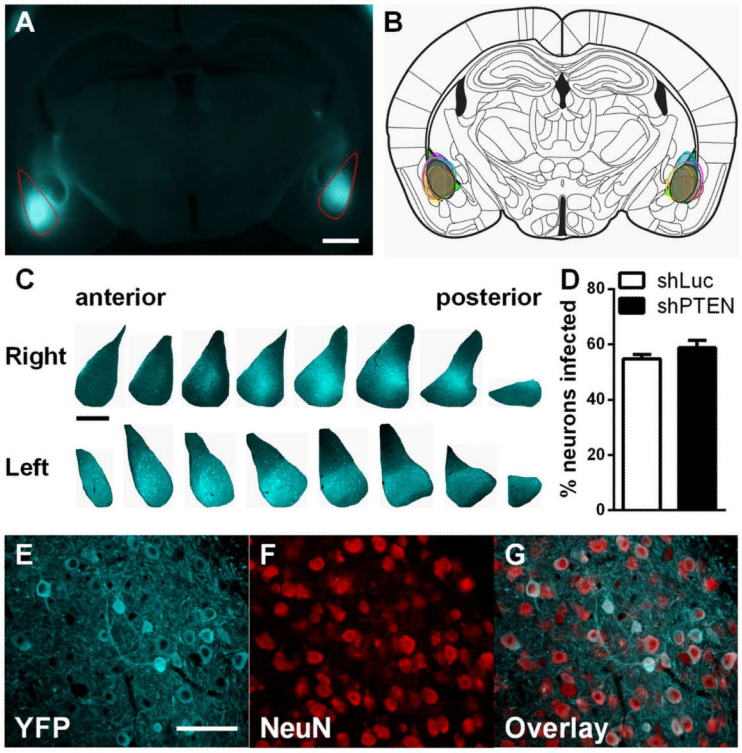

Figure 1. shPTEN and shLuc virus injections target the basolateral amygdala complex

A. Example image of bilateral infection of the BLA (outlined in red). **B.** A schematic of a coronal mouse brain section at −1.70 mm relative to bregma (adapted from Paxinos and Franklin 2001). The BLA is shaded in with bright green. Each oval color represents the viral spread within a single shLuc mouse that was used in behavioral experiments. **C.** Sections of virally infected BLA (sections separated by 180 Nm) showing anterior-posterior spread of virus. **D.** Quantification of cell counts reported as the percentage of NeuN+ cells that were also YFP+. No difference between groups was observed using a student's t-test. N = 3 mice for both shPTEN and shLuc groups. **E–G.** Representative images of immunofluorescent staining of YFP (cyan) and NeuN (red). Images were taken within a virally infected region of the BLA and the number of NeuN+ and YFP+ cells were counted. (scale bar in **A** = 1mm; scale bar in **C** = 500 μm and applies to all images in panel C; scale bar in **E** = 60 μm and is applicable to **E–G**.)

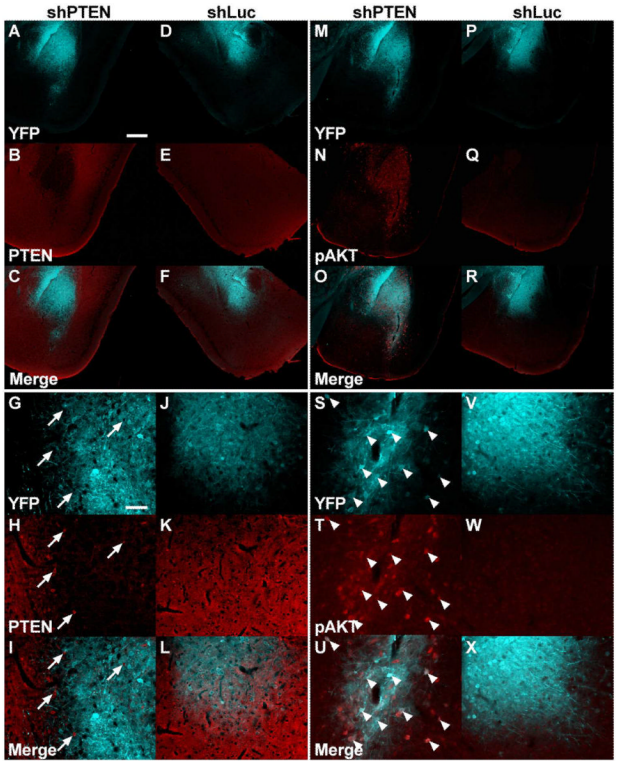

Figure 2. shPTEN infected cells experience a robust decrease in PTEN expression and a resultant increase in phosphorylated AKT

A–L are double immunofluorescent staining of YFP (cyan) PTEN (red). shPTEN infected cells exhibit a dramatic decrease in PTEN expression levels (**A–C low power and G–I high power**) while shLuc infected cells do not decrease PTEN expression (**D–F low power and J–L high power**). Arrows point to cells within or at the borders of the infected region that still express PTEN and are not YFP positive. **M–X** are double immunofluorescent staining of YFP (cyan) and phosphorylated AKT (pAKT, red). shPTEN infected cells display upregulated levels of pAKT (**M–O low power and S–U high power**) while shLuc infected cells do not express significant levels of pAKT (**P–R low power and V–X high power**). Arrowheads point to individual cells that are double positive for YFP and pAKT. (Scale bar in **A** = 500 μm and is applicable to images **A–F and M–R**; scale bar in **G** = 100 μm and is applicable to images **G–L and S–X**.)

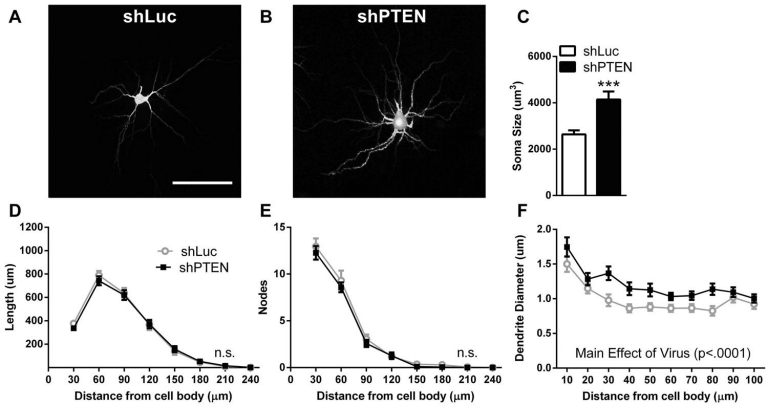

Figure 3. Soma size and dendrite width are increased in shPTEN infected cells compared to shLuc infected cells in the BLA

A and B. Representative images of shLuc (A) and shPTEN (B) infected neurons filled with the red Fluor 568 fluorescent dye. **C.** Quantification of 3-dimensional soma size (μm^3) was analyzed after 3-D reconstruction of neurons using Neurolucida. **D and E.** A Scholl analysis was performed on 3-D reconstructions of Alexa Fluor 568 filled neurons using concentric circles whose radii increased incrementally by 30 μm. There was no difference in length of dendrites (**D**) or intersections of dendrites with concentric circles (**E**). **F**. Dendrite diameter was measured in 10 μm increments. One dendritic segment was pseudo-randomly chosen and measured for each neuron at each distance. (N=17 shLuc infected neurons and N=16 shPTEN infected neurons; Scale bar in **A** = 100 μm and is applicable to **A** and **B**; ***p<0.001; n.s. = not significant)

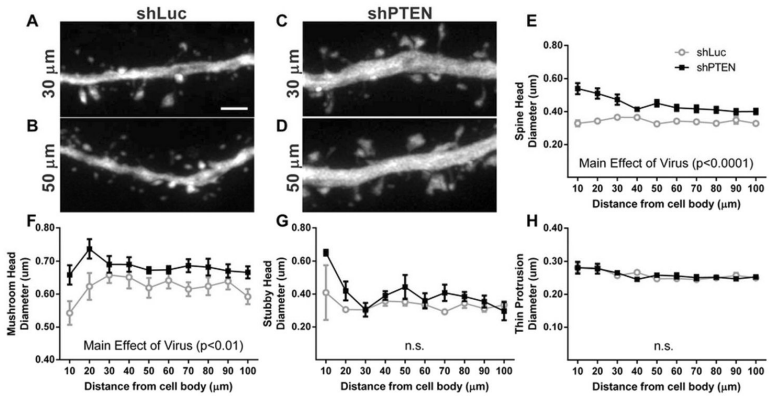

Figure 4. Mushroom spine head diameter is significantly increased in the shPTEN infected neurons

A–D. Representative images of Alexa Fluor 568 filled dendritic segments from shLuc infected (**A and B**) and shPTEN infected (**C and D**) neurons at 30 μm and 50 μm away from the cell body. **E.** Average spine head diameter is increased in shPTEN infected neurons compared to shLuc infected neurons. A detailed analysis of spine subtypes reveals that this increased spine head diameter is due to an increase in mushroom spine head diameter (**D**) while stubby spines (**E**) and thin protrusions (**F**) show no increase in spine head diameter. (N = 17 shLuc infected neurons and N = 16 shPTEN infected neurons. Scale bar in **A** = 2.5 μm and is applicable to **A–D**. n.s. = not significant)

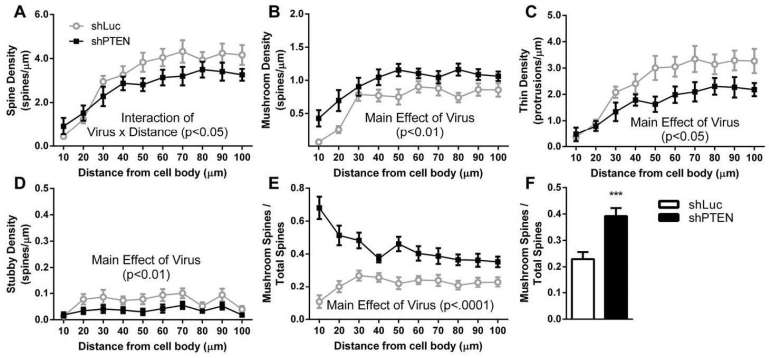

Figure 5. Fraction of mushroom spines is increased in shPTEN infected cells

A. Spine density is decreased in more distal dendrite segments. **B–D.** An analysis of spine subtypes reveals that although thin protrusions (**C**) and stubby spines (**D**) account for the decrease in total spine density, mushroom spine density (**B**) is significantly increased. **E.** There is a significant shift toward an increased fraction of mushroom spine density, particularly in the more proximal dendrite segments. **F.** The total mushroom spine density fraction including all distances from the cell body is increased in the shPTEN infected neurons compared to controls. (N = 17 shLuc infected neurons and N = 16 shPTEN infected neurons; ****$p < 0.0001$)

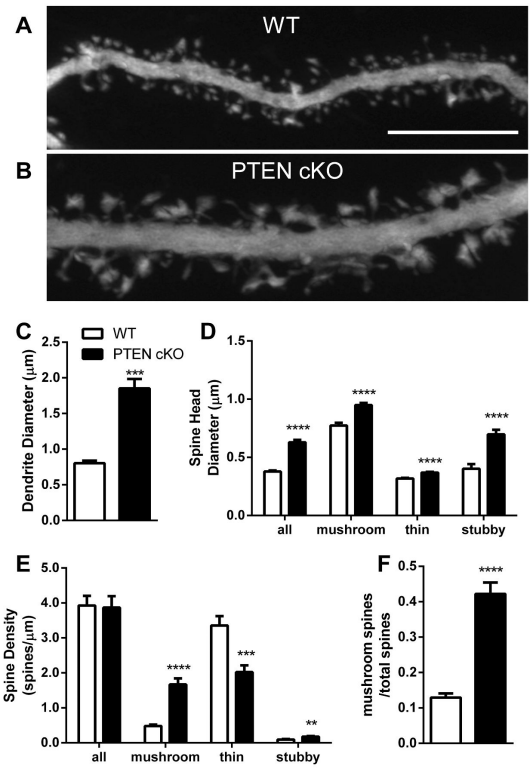

Figure 6. Conditional PTEN KO mice selective for the dentate gyrus granule neurons have increased mushroom spine head diameter and an increase in the mushroom spine fraction with no change in total spine density

A and B. Representative images of Lucifer Yellow filled WT (A) and PTEN-cKO (B) dentate gyrus granule neuron dendritic segments taken 20–50 μm from the dentate gyrus cell body layer. **C.** Diameter of the dendritic segments used for spine analysis. **D.** Average spine head diameter of all spine types, mushroom spines, thin protrusions and stubby spines. **E.** Spine density of all spine types, mushroom spines, thin protrusions and stubby spines. **F.** Quantification of the mushroom spine fraction. (N=17 for both WT and PTEN-cKO neurons; **p < 0.01; ***p < 0.001; ****p < 0.0001; Scale bar in **A** = 10 μm and is applicable to **A** and **B**)

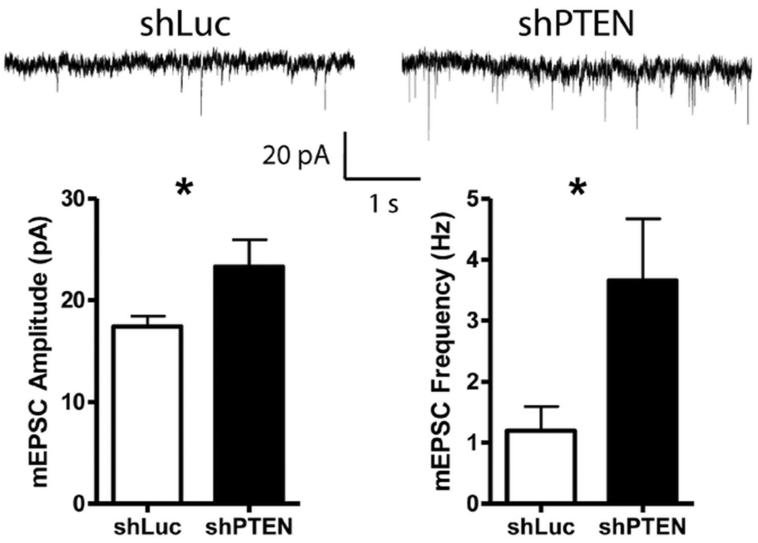

Figure 7. shPTEN infected neurons show increased miniature EPSC amplitude and frequency

Top. Representative traces from shLuc and shPTEN mEPSC recordings. Bottom Left. Increased amplitude of mEPSCs in shPTEN compared to shLuc infected BLA neurons. Bottom Right. Increased mEPSC frequency in shPTEN compared to shLuc infected BLA neurons. (*$p < 0.05$; N = 11 shLuc and N = 10 shPTEN)

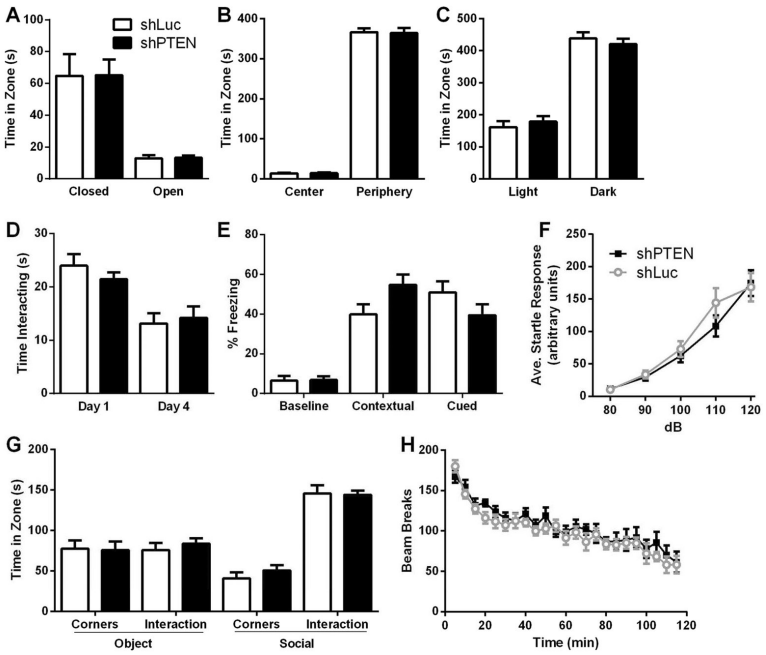

Figure 8. shPTEN injected mice do not show behavioral phenotypes three weeks post-injection

No difference was observed between shPTEN and shLuc injected mice in three tests of anxiety: elevated plus maze (**A**), open field (**B**) and dark/light box (**C**). Additionally, no differences were observed in social interaction with a juvenile (**D**), both contextual and cued fear conditioning (**E**), startle threshold (**F**), social interaction in the open field (**G**) and locomotion (**H**). (N = 12 shLuc mice and N = 15 shPTEN mice)

Table 1

Description of primary antibody specificity and source.

Antibody	Type	Host	Immunogen	Dilution	Source	Catalog No.	JC Antibody Registry ID
Anti-GFP	Polyclonal	Rabbit	Purified GFP from Jellyfish Aequorea Victoria	1:2000	Invitrogen	A6455	AB_22150
Anti-GFP	Polyclonal	Chicken	Purified Recombinant GFP	1:2000	Aves Labs	1020	AB_10000240
Anti-NeuN	Monoclonal	Mouse	Purified cell nuclei from mouse brain	1:250	Chemicon	MAB377	AB_2298772
Anti-PTEN	Monoclonal	Rabbit	Epitope surrounds amino acid 395 of PTEN sequence	1:400	Cell Signaling	9188	AB_2174349
Anti-pAKT	Monoclonal	Rabbit	Epitope surrounds serine 473 of AKT sequence	1:200	Cell Signaling	4060	AB_916027

(Abbreviations: JCN – Journal of Comparative Neurology; GFP – Green Fluorescent Protein).